Spectroscopic Investigations and Molecular Dynamics Studies of Cationic Exchanged EMT Zeolites

Daniel Bougeard, Claude Brémard,* Denis Dumont, and Marielle Le Maire

Laboratoire de Spectrochimie Infrarouge et Raman, UMR-CNRS 8516, Centre d'Etudes et de Recherches Lasers et Applications, Université des Sciences et Technologies de Lille I, Bâtiment C5, 59655 Villeneuve d'Ascq Cédex, France

Jean Marie Manoli and Claude Potvin

Laboratoire de Réactivité de Surface, UMR-CNRS 7609, Université Pierre et Marie Curie, 4, Place Jussieu, 75252 Paris Cédex 05, France

Received: May 19, 1998; In Final Form: October 20, 1998

Significant Raman and infrared spectra of the fully dehydrated and bare hexagonal M_{20}EMT zeolites (M = Li^+, Na^+, K^+, Rb^+, Cs^+, NH_4^+, and H^+) have been obtained particularly in the low-frequency region, at room and low temperature. The vibrational properties of M_{20}EMT were found to be analogous to those of cubic M_{40}FAU with identical aluminum content. However, significant changes in position and intensity of the bands assigned to the framework vibrations were observed according to the nature of the extraframework charge-balancing cation of the exchanged zeolites. Molecular dynamics calculations were used to model the vibrational features of the M_nEMT (n = 0 or 20; M = Na^+ or K^+) framework and extraframework cations. The main features of both the IR and Raman spectra were reproduced in the mid as well as in the low-frequency ranges. The results of the calculations demonstrate that the cation vibrations significantly participate in the spectral range from 20 to 250 cm^{-1} for all cation sites and are in accurate agreement with the infrared and Raman features assigned to the cation motions. The data of the molecular dynamics simulations of the window fluctuations in the M_nEMT zeolites show that the aluminum content and extraframework cations affect both the size and the amplitude of the fluctuations of the windows in the zeolite, although the cations are not located in the windows. The calculated spectral densities of the window fluctuations show the most prominent peaks around 100 cm^{-1} and are in agreement with the low-frequency Raman features observed around 100 cm^{-1}.

Introduction

The faujasitic family of zeolites plays an important role in a wide variety of separation, chemical, and petrochemical processes. Particulary zeolites with the cubic faujasite (FAU) topology are established acid catalysts for several large-scale refinery processes. The FAU structure is built from "sodalite units" or cubooctahedra, which are linked together through hexagonal prisms called double-6-ring (D6R). A high silicon content of the framework improves its thermal and hydrothermal stability and provides efficient catalytic performances. Inorganic synthesis allows the preparation of a FAU zeolite with an Si/Al ratio less than 2.7. High-silica faujasite samples are commonly prepared by postsynthesis dealumination treatments.[1] Organic additives (15-crown-5 ether) can also increase the silicon content of the as-synthesized zeolite products with a Si/Al ratio higher than 2.7, but less than 4.[2−4]

The organic molecules sometimes act as a structure directing agent; the substitution of 15-crown-5 ether (15C5) for 18-crown-6 (18C6) in the hydrogel leads to the crystallization of a silicon-rich EMT structure, which is a hexagonal variant of the cubic FAU structure.[2−4] The as-synthesized Na_nEMT or Na_nFAU zeolite contains occluded 18C6 or 15C5, respectively.[2−5] Na^+ extraframework cations equilibrate the charges arising from the aluminum sites of the framework. The removal of the organic matter and water of the as-synthesized products provide bare Na_nEMT or Na_nFAU structure. Due to the different linking of sodalite cages, the microporous structures of the EMT and FAU framework are substantially different.[5−12] The cubic FAU structures exhibit one type of supercage. The 1.3-nm diameter supercage is accessed through four 0.75-nm free diameter circular apertures. The structures, the cation site occupancy, the spectroscopic properties, as well as the computer modeling study of the FAU zeolites have been extensively described in a wide range of composition, practically from Si/Al = 1 to 1000,[1,8,9,13−29] whereas for the structural and spectroscopic properties of the hexagonal EMT zeolites the same level of knowledge has not been reached today.[2−12,30−39]

In the EMT framework two different types of supercages are present in equal number. The largest supercages have free dimensions of 1.3 × 1.3 × 1.4 nm^3 and are accessed through two circular and three elliptical apertures. The circular apertures with a free diameter of 0.85 nm connect the largest supercages, while the elliptical apertures with free dimensions of 0.54 × 0.74 nm^2 connect both cage types. The smallest supercages have free dimensions of 0.7 × 1.3 × 1.3 nm^3 and can be entered through the three elliptical windows. From previous diffraction and ^{23}Na NMR spectroscopic data the charge-balancing Na^+ cations are localized in different sites with partial occupancy.[5,6,32] These extraframework cations can be exchanged for specific purposes by other cations without altering the framework structure.[33,35,38,39]

10.1021/jp982298+ CCC: $15.00
Published on Web 12/08/1998

For the optimization of many applications a detailed knowledge of the adsorption and diffusion behavior of guest molecules in zeolite channels is essential.[40,41] These properties mainly depend on the size of the windows connecting the cavities and the size and the occupancy of the extraframework cations of the zeolites, but the diffusion also depends on the flexibility of the framework and the dynamics of the extraframework cations.[21,42,43] The static geometrical parameters are usually available from diffraction data;[5,6] however, the dynamical information about the zeolite lattice and particularly of the windows and the cations can be deduced from vibrational data. The essential step in interpreting vibrational spectra, namely, infrared absorption and Raman scattering in the present work, is the assignment of experimentally obtained bands to normal modes. As this cannot easily be achieved on a purely empirical basis, computer simulation techniques, such as molecular dynamics and normal modes analyses, can be used to elucidate the problem of framework and cation vibrations in the vibrational spectra of zeolites.[37]

In the present work we report the chemical characterization and the infrared and Raman spectra of bare M_nEMT zeolites, (M = Li^+, Na^+, K^+, Rb^+, Cs^+, NH_4^+, and H^+) recorded in the mid- and low-frequency regions at room as well as low temperature. The aim of the present paper is to show that the use of the molecular dynamical calculations, based on an atom−atom force field for the cation-framework interaction, can describe the main structural and vibrational features of M_nEMT zeolites (M = Na^+ or K^+; n = 0 or 20). This is done by comparing the calculated structures as well as infrared and Raman spectra to the experimental data. The emphasis of the present work was set on the zeolitic window fluctuations and on the extraframework cation motions which appear to be in close relation with the specific diffusion properties of the EMT zeolites

Experimental Section

1. As-Synthesized Zeolites. The silicon-rich EMT and FAU samples were obtained according to the procedure previously described,[2,3] using the same reactants: sodium aluminate (Carlo Erba 56% Al_2O_3, 37% Na_2O), colloidal silica (CeCa 40% SiO_2, 60% H_2O), sodium hydroxyde (Prolabo Normapur, 98%). 18C6, 1,4,7,10,13,16-hexaoxacyclooctadecane and 15C5, 1,4,7,10,13-pentoxacyclopentadecane, were purchased from Aldrich.

The EMT zeolite was synthesized by using a starting mixture with the following molar composition; 10 SiO_2:1 Al_2O_3:2.4 Na_2O:1 18C6:140 H_2O. The FAU zeolite was synthesized by using a starting mixture with the following molar composition; 10 SiO_2:1 Al_2O_3:2.4 Na_2O:15C5:140 H_2O. The gel was stirred for 48 h. The final reaction mixture was heated in Teflon lined stainless steel autoclaves for eight days at 100 °C. The resulting products were collected by filtration.

The ^{29}Si NMR spectroscopy, the elementary analyses, and thermal analyses of the as-synthesized samples correspond to the following formulas per unit cell EMT = $Na_{19}(SiO_2)_{77}(AlO_2)_{19}$-$(C_{12}H_{24}O_6)_4$·45 H_2O and FAU = $Na_{40}(SiO_2)_{152}(AlO_2)_{40}$-$(C_{10}H_{20}O_5)_8$·100 H_2O. The purity of the EMT and FAU phases were checked by X-ray powder diffraction (XRD).

2. Calcination and Cation Exchange. The removal of the organic matter of the as-synthesized products was realized by heating the compound stepwise in air up to 773 K and then under flowing pure O_2 at 773 K. The removing of the organic matter was controlled through a temperature programmed desorption experiment. The Na_{19}EMT and Na_{40}FAU samples were cooled to room temperature and held in moist atmosphere.

The Na^+ cations of Na_{19}EMT have been completely exchanged by Li^+, K^+, Rb^+, Cs^+, and NH_4^+ cations. The exchange was carried out according to the processes already used for FAU zeolites.[25] The elementary analyses correspond to the following formula per EMT unit cell: $Li_{17}Na_2(SiO_2)_{77}(AlO_2)_{19}$, Na_{19}-$(SiO_2)_{77}(AlO_2)_{19}$, $K_{18}Na(SiO_2)_{77}(AlO_2)_{19}$, $Rb_{16}Na_3(SiO_2)_{77}$-$(AlO_2)_{16}$, $Cs_{16}Na_3(SiO_2)_{77}(AlO_2)_{19}$, $(NH_4)_{18}Na(SiO_2)_{77}(AlO_2)_{19}$, $H_{18}Na(SiO_2)_{77}(AlO_2)_{19}$.

3. Dehydration. The powdered hydrated zeolite sample was introduced into an evacuable heatable silica cell. The sample was dried under vacuum (10^{-3} Pa) and heated stepwise to 773 K. O_2 was then admitted into the cell. A thermal gravimetric analysis showed that this temperature is sufficient to remove all water molecules. The crystallinity of the samples checked by XRD was not reduced by this treatment. After 6 h the sample was held under vacuum and cooled to room temperature. Then the powder was transferred under dry argon into a cylindrical thin glass tube which was sealed off for the dispersive Raman experiments. The powder was transferred under dry argon in a quartz glass Suprasil cuvette for FT-Raman experiments.

Before any in situ IR absorption measurements the samples supported on a silicon disk were freshly dehydrated under vacuum within heatable evacuable cells. The dehydration level was checked through the intensity of the infrared bands of occluded water molecules.

4. Instrumentation. The elemental analyses of the bulk solids were obtained from the Service Central d'Analyse du Centre National de la Recherche Scientifique (Vernaison, France). The exchange of the cations was systematically verified by EDX analysis. Zeolite grains to be studied by STEM-EDX were dispersed in pure ethanol; the suspension was stirred in an ultrasonic bath, and one drop was placed on a carbon-coated copper grid. The specimens were studied using a JEOL (JEM 100CXII) transmission scanning electron microscope equipped with a scanning device ASID 4D (STEM mode). The operating voltage was 100 kV. EDX analyses were performed using a LINK AN10000 system connected to a silicon−lithium diode detector and a multichannel analyzer. The X-rays emitted from the specimen upon electron impact were collected in the 0−20 keV range for 250 s. The X-ray EDX analyses were obtained from large domains (e.g., 120 × 160 nm^2 to 300 × 400 nm^2). The atomic composition was obtained with the 2 LINK program (RTS-2/FLS).

A Siemens D500 automatic diffractometer with a Cu Kα monochromatized radiation source was used to record the X-ray diffraction (XRD) patterns of the several solid phases.

Thermogravimetric analyses (TGA) and differential thermal analyses (DTA) profiles were recorded on a Setaram TGA 92 thermobalance in oxygen/helium atmosphere. The temperature programmed desorption was performed using quadrupole mass spectrometer Delsi Anogaz 200.

The ^{29}Si MAS NMR spectra were recorded using Bruker MSL 400 (at 79.5 MHz) spectrometer. The ^{29}Si MAS NMR spectra were recorded with 2 μs radio frequency pulses, 10 s recycle delays using rotor spinning rate of 5 kHz and accumulation of 2000 to 20000 scans. The ^{29}Si chemical shifts are quoted in ppm from external tetramethylsilane. The spectra simulations were obtained using an extended version of WINFIT software (Bruker). The framework Si/Al molar ratio was given by Si/Al = ΣISi(nAl)/$\Sigma n/4I$Si(nAl), where ISi(nAl) is the intensity of the NMR signal assigned to the Si(nAl) units.

The IR absorption spectra of the zeolites were recorded under in situ conditions using the diffuse transmission technique

through a Bruker IFS 113V instrument equipped with liquid N_2-cooled MCT detector or a liquid He-cooled bolometer. Mid-IR spectra (4000−500 cm^{-1}) were recorded using a cell equipped with KRS-5 windows, whereas far-IR spectra (500−50 cm^{-1}) were recorded using a cell equipped with silicon windows. The Opus Bruker software was used for spectral acquisition, data treatment and plotting.

The low-frequency Raman spectra were recorded by using the dispersive technique at 300 and 77 K in the 50−600 cm^{-1} wavenumber range on a triple-monochromator spectrometer DILOR Model RTI equipped for accumulation of spectra. The Raman scattering was excited using argon or krypton laser lines (457.9, 488.0, 514.5, 568.2, and 647.9 nm) and a laser power of 400 mW was used; all spectra reported in the figures correspond to the 568.2 nm excitation. With the backscattering geometry and a careful focalization of the laser beam on a point inside the zeolite samples, the Raman spectrum of the glass tube is reduced to a negligible level. Slit widths were typically 4 cm^{-1}, and the sloping background in the Raman spectra was not corrected with pretreated samples; the careful sample preparation avoids the apparition of any fluorescence. To reduce the strong "Rayleigh band" in the lower wavenumber region, narrower slit widths were used. The laser parasite lines can interfere with the low-frequency Raman bands of the sample under study. To detect the significant Raman bands of the sample, the Raman spectra were recorded with all the available exciting radiations and carefully compared in the Stokes and anti-Stokes regions, at 300 and 77 K. The Raman spectra using the FT technique were recorded at room temperature on a Bruker spectrometer Model IFS 88, with a NIR Nd^{3+}:YAG laser at 1064 nm as excitation source. The laser power was 400−700 mW. The spectra were recorded at 4 cm^{-1} resolution using 200 scans.

Crystal Structures and Factor Group Analyses. The structures of the dehydrated $H_1Na_{21}(AlO_2)_{22}(SiO_2)_{74}$,[6] dehydrated $H_{12}Na_{10}(AlO_2)_{22}(SiO_2)_{74}$6, and partially dehydrated $H_{12}Na_8(AlO_2)_{20}(SiO_2)_{76}$5 EMT zeolites are available in the literature through X-ray powder diffraction study using the Rietveld refinement procedure. XRD experiments showed that the present calcined and exchanged materials have a hexagonal EMT framework topology with hexagonal ABAB stacking of sodalite cage layers. With the $P6_3/mmc$ or D_{6h} space group the Si/Al distribution was assumed to be at random. The siting pattern of Si and Al atoms in the EMT zeolites was recently determined by a combination of ^{29}Si MAS NMR[8] and model generation by computer algorithm.[44] A model of random Al siting[45] obeying the Loewenstein rule (absence of Al−O−Al linkages) is not in complete agreement with the experimental Al/Si distribution whereas a zoned Al/Si ordering model yields an accurate agreement.[44]

This zoned model was used to explain the population of sodium cations at the different cations sites in NaEMT sample.[46] Table 1 shows the observed and calculated occupation numbers for extraframework Na^+ cations for EMT zeolites taken in the literature.[5,6,32,46] To determine the spectral activity of the extraframework cations the full occupancy of the available cation sites was assumed. The sites I_a and I_b are assumed to be empty. The representation of the cationic degrees of freedom classify as shown in Table 2.

The structures of the partially dealuminated $Na_5H_4(SiO_2)_{183}(AlO_2)_9$, $Na_7H_{11}(SiO_2)_{174}(AlO_2)_{18}$, and $Na_{14}H_{14}(SiO_2)_{164}(AlO_2)_{28}$ FAU zeolites are available in the literature.[47] The representation of the cationic degrees of freedom classify as shown previously.[25]

TABLE 1: Occupation Numbers for Extraframework Cation Sites I_{ab}, I'_{ab}, and II_{ab} in NaEMT Zeolites (Space Group $P6_3/mmc$)

EMT zeolite	I_a (6g)	I_b (2c)	I'_a (12k)	I'_b (4f)	II_a (12k)	II_b (4f)	T (K)	ref
$Na_{21}H_1(AlO_2)_{22}(SiO_2)_{74}$	1.5	0	4.4	4.6	6	3	723	6
$Na_{21}H_1(AlO_2)_{22}(SiO_2)_{74}$	1.7	0	4.4	4	5.4	3	723	46
$Na_{20}(AlO_2)_{20}(SiO_2)_{76}$[a,b]		2	6	2	6	2	50	5
$Na_8H_{12}(AlO_2)_{20}(SiO_2)_{76}$[b]			3		4	1.3	293	5
$Na_{10}H_{12}(AlO_2)_{22}(SiO_2)_{74}$	2.5		3.5	3.3	2.4	1.6	723	6
$Na_{10}H_{12}(AlO_2)_{22}(SiO_2)_{74}$	2.0	0	2.5	3.9	2.5	1.9	723	46
$Na_{20}(AlO_2)_{20}(SiO_2)_{76}$	0.5		19.9				300	32

[a] With 4 18C6 per unit cell. [b] Partially hydrated.

TABLE 2: Factor Group Analyses of the Translational Motions of the Extraframework Cations in the EMT Zeolites (Space Group $P6_3/mmc$ or D_{6h})

	contributing symmetry species and optical activity
site $II_a-I'_a$ (12k) $C_s = m$	$2A'(x,y)$, $A''(z)$
factor group D_{6h}	$2\,A_{1g} + 2\,A_{2g} + B_{1g} + B_{2g} + 2\,E_{1g}(R) + 4\,E_{2g}(R) + A_{1u} + A_{2u}(IR) + 2\,B_{2u} + 4\,E_{1u}(IR) + 2\,E_{2u}$
site $II_b-I'_b$ (4f) $C_{3v} = 3m$	$E(x,y)$, $A_1(z)$
factor group D_{6h}	$A_{1g}(R) + B_{2g} + E_{1g}(R) + E_{2g}(R) + A_{2u}(IR) + B_{1u} + E_{1u}(IR) + E_{2u}$
site I_a (6g) $C_{2h} = 2/m$	$2B_u(x,y)$, $A_u(z)$
factor group D_{6h}	$A_{1u} + A_{2u}(IR) + 2\,B_{1u} + 2\,B_{2u} + 4\,E_{1u}(IR) + 2\,E_{2u}$
site I_b (2c) $D_{3h} = 6m2$	$E'(x,y)$, $A_2''(z)$
factor group D_{6h}	$B_{2g} + E_{2g}(R) + A_{2u}(IR) + E_{1u}(IR)$

Calculations. A simulation box containing one unit cell of Na_{20}EMT zeolite (76 Si, 20 Al, 192 O, and 20 Na atoms) was used in the MD calculations. Although the dimension of the box along the x and y axis were smaller than twice the cutoff radius used in the Coulombic interactions, the dynamic behavior of the cations is not significantly different from the cation calculations with four unit cells (two along x and y axes). The initial atomic coordinates and cation site occupancy were taken in the crystallographic positions of the Na_{20}EMT.[5,6] First a random procedure was used to distribute the cations over the extraframework sites with partial occupancy deduced from diffraction data, second the substitutional Si, Al disorder was applied according to the Loewenstein rule. Models taking into account the zoned Si/Al ordering model[44] were also considered in order to evaluate the influence of the Si/Al distribution on calculated spectra. As the differences turned out to be small, other distributions schemes such as the Melchior model,[47] up to now only applied to the FAU topology, were not tested. Assuming that the Na_{20} and K_{20}EMT zeolite frameworks are analogous, the initial geometry of K_{20}EMT was obtained by replacing Na atoms by K atoms. After an equilibrating period the framework geometries were found to be in the expected ranges. No diffusion of the cations occurred during the equilibration period, as well as during all further calculations. For the purely siliceous form of the zeolite we used the Si, Al, and O atomic positions of the Na_{20}EMT geometry as starting structure and replaced Al atoms by Si. The resulting purely siliceous EMT framework structure exhibited smaller changes than the experimental error from the experimental structure of Na_{20}EMT.

The MD simulations of dispersely packed cations were performed with a simulation box containing one unit cell of dealuminated Na_nFAU zeolites (n = 8, 18, and 28). The initial atomic coordinates were the crystallographic positions of the Na_nH_mFAU structures.[48] First, a random procedure was used

to distribute the cations over the extraframework sites with partial occupancy deduced from diffraction data taking into account the substitution of H^+ by Na^+; second, the substitutional Si, Al disorder was applied according to the Loewenstein rule. No attempt using other distributions schemes such as the Melchior model[47] was undertaken yet.

The previously reported simplified general valence force field (SGVFF) was used to calculate the interactions between the atoms of the framework,[49] whereas the cation framework interactions were described through an equation including Coulombic potential, repulsion, and dispersion terms.[49] The values of the SGVFF force constants are given in reference.[22,43] The framework−cation interaction terms was described with the following equation:

$$V_{\mathrm{FW-C}} = \frac{q_i q_j}{r_{ij}}\left(1 + \frac{\mathrm{sign}(q_i q_j)}{n+1}\frac{(s_i + s_j)^n}{r_{ij}^n}\right) + V_{\mathrm{D}} \qquad (1)$$

where q_i, q_j, s_i, and s_j are the atomic charges and ionic radii for ions i and j, respectively. The first term in parentheses corresponds to the pure Coulombic potential. The second one represents the repulsion of the core electrons and V_D is a dispersion term ($V_D = C_{ij}/r_{ij}^6$). The sign is the usual sign function. The value of the parameter n is equal to nine. The C_{ij} constants for the dispersion term were calculated as previously described.[49]

The equations of motions were integrated by using the velocity form of the Verlet algorithm with a time step of 0.2 fs. The simulations were performed at 300 K in the NVE ensemble for at least 100 ps. The details of the calculations used throughout this work are analogous to those recently reported.[49] All dynamical properties are already converged with a cutoff distance of 10 Å. Therefore this distance was applied and like in ref 49 the time-consuming Ewald summation was not performed. The densities of vibrational states of individual atoms (Si, Al, O, Na, and K) and of the system were calculated by Fourier transformation of the corresponding velocity autocorrelation function. The calculated spectral resolution is 2 cm^{-1}. The infrared spectra were calculated by Fourier transformation of the autocorrelation function of the total dipole moment of the system. Infrared intensities were calculated assuming that the charges +1.3, +1.1, −0.8, and +1 e^- on the atoms Si, Al, O, and *M*, respectively, remain constant throughout the vibrational motions. This simplified model was adopted since it requires the minimum number of input parameters. The Raman spectra were calculated from the autocorrelation function of the polarizability according to a procedure previously described.[50] The autocorrelation function of the polarizability is estimated from the position of the atoms by a simplified method using only the derivative of the polarizability with respect to the bond length for each type of bond[19] and neglecting the transversal components of the α polarizability tensor. As only relative intensities are considered the derivatives $d\alpha/dr$ for Si−O and Al−O linkages were considered in a ratio 1:0.75, such as for zeolite A.[49] As an approximation of the disorder of the microcrystals of the powdered samples, the Raman intensity was then calculated with the help of the formulas valid for liquids and assuming a space and time averaging of the molecules. This approximation leads to an overestimation of the anisotropic part of the Raman scattering, particularly over 700 cm^{-1}.[49,50] For all the spectra we took the mean value of the spectra of 10 simulations with different initial conditions; this procedure permits a better sampling of the phase space and a distribution of energy over the normal modes corresponding to the Boltzman distribution, thus leading to a reproductibility in the order of 10% for the calculated Raman intensity.

Two aspects of the window flexibility were examinated, the characteristic dimensions and the area, respectively. The diameter d of the circular window is defined by the distance between two O atoms located at opposite positions in the 12-membered rings. As an appropriate measure of the window area, we chose the area *S* of the hexagon defined by the six O atoms of the circular window. We can approximate the area of the hexagon as a function of the three corresponding instantaneous diameters of the 12-membered ring.[21] The main axes *D* and *d* of the elliptic window are defined by the largest and shortest distance between the two O atoms located at opposite positions in the 12-membered ring, respectively. The area of the elliptic window can be evaluated as $\pi dD/4$. To obtain information about the frequencies involved in the dimensions of the window fluctuations, their spectral density was computed as Fourier transformation of the diameter and main axes autocorrelation function:[43]

$$C_d(t) = 1/T < [\mathrm{d}(t') - d_{\mathrm{m}}][d(t'+t) - d_{\mathrm{m}}] \qquad (2)$$

where d denotes current and d_m the mean value of the characteristic distance. The averaging occurs over all O pairs.

Results and Discussion

Before the obtention of reliable mid-IR and far-IR absorption spectra and Raman scattering spectra corresponding to the vibrational motions of the framework and extraframework cations of pure dehydrated bare M_nEMT zeolites some key experimental problems have been resolved (see Experimental Section). All experimental data (elementary analyses, ^{29}Si MAS NMR, XRD, and vibrational spectroscopic data) are in accurate agreement with bare dehydrated M_nEMT zeolites. To obtain an accurate comparison between the vibrational properties of hexagonal EMT and cubic FAU zeolites, the Na_{20}EMT and Na_{40}FAU zeolites were synthesized with identical starting chemical mixtures except the template molecule 18C6 and 15C5, respectively (see Experimental Section). The calcination, hydration, and dehydration procedures provide pure dehydrated bare Na_{40}FAU (Si/Al = 3.8) zeolite with identical chemical composition as found for bare Na_{20}EMT (Si/Al = 3.8). However, the comparison of the vibrational spectra of the exchanged M_nEMT zeolites was made with the previously reported vibrational spectra of M_{56}FAU zeolites (Si/Al = 2.4), although the chemical compositions are somewhat different.[15,23,25]

1. Infrared Absorption Spectra. The spectra obtained after dehydration at 773 K and subsequent cooling of the bare M_{20}EMT samples $M^+ = Li^+$, Na^+, K^+, Rb^+, and Cs^+ are presented in Figures 2 and 3 for the 1550−500 and 700−100 cm^{-1} ranges, respectively.

In the first region, the asymmetric (850−1350 cm^{-1}) and the symmetric (650−850 cm^{-1}) Si−O and Al−O stretching modes are observed as intense bands. In the second region the O−Si/Al−O and Si/Al−O−Si bending modes (250−620 cm^{-1}) are observed as well as the cation translational motions in the lower frequency region (50−300 cm^{-1}).

It is tempting to compare the IR absorption spectra of hexagonal M_{20}EMT and cubic M_nFAU zeolites. The in situ calcination of the as-synthesized Na_{20}EMT(18C6)$_4$ or Na_{40}FAU-(15C5)$_8$ zeolite generates bare dehydrated Na_{20}EMT or Na_{40}-FAU zeolite with identical chemical composition, $Na_{20}(SiO_2)_{76}$-$(AlO_2)_{20}$, or $Na_{40}(SiO_2)_{152}(AlO_2)_{40}$, per unit cell, respectively. The calcined Na_{20}EMT and Na_{40}FAU zeolites are well-crystallized in pure hexagonal and cubic phases, respectively,

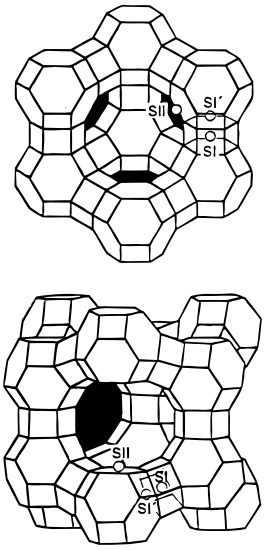

Figure 1. Structure of FAU zeolite and cation sites SI, SI′, SII (top) and EMTzeoliteand cation sites SI(a,b), SI′(a,b), SII (a,b) (bottom).

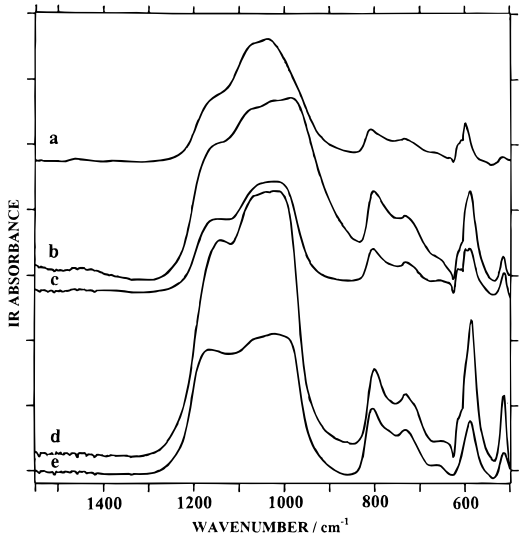

Figure 2. Experimental IR spectra (1500−500 cm^{-1}) of dehydrated M_{20}EMT zeolites: (a) Li_{20}EMT, (b) Na_{20}EMT, (c) K_{20}EMT, (d) Rb_{20}EMT, (e) Cs_{20}EMT.

as demonstrated by the X-ray diffraction patterns.[7] The mid-frequency IR absorption of the hexagonal Na_{20}EMT and cubic Na_{40}FAU samples were found to be similar.[34] However, some weak but significant differences can be observed on the vibrational spectra.

The far-IR spectra are expected to provide evidence of the vibrational motions of the extraframework Na^+ cations below 200 cm^{-1}. The far-IR spectra of the Na_{20}EMT and Na_{40}FAU zeolites are shown in Figure 4 and exhibit weak but marked differences between the two zeolites with identical composition.

It should be noted that a supplementary hydration-dehydration treatment of both zeolites generates far-IR spectra markedly different from those obtained through calcination of the as-synthesized products, and they suggest some rearrangement of the cation site occupancy. For FAU zeolites the supplementary treatment yields better structured spectra which could correspond to a less disordered cationic distribution. This issue is less evident for EMT zeolites.

The main trends in the IR spectra of the M_{20}EMT zeolites are analogous to the corresponding M_{56}FAU zeolite spectra, respectively, although the chemical compositions are somewhat

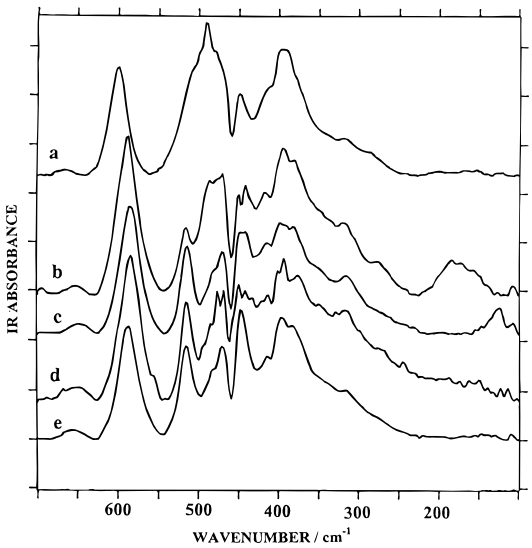

Figure 3. Experimental IR spectra (700−100 cm^{-1}) of dehydrated M_{20}EMT zeolites: (a) Li_{20}EMT, (b) Na_{20}EMT, (c) K_{20}EMT, (d) Rb_{20}EMT, (e) Cs_{20}EMT.

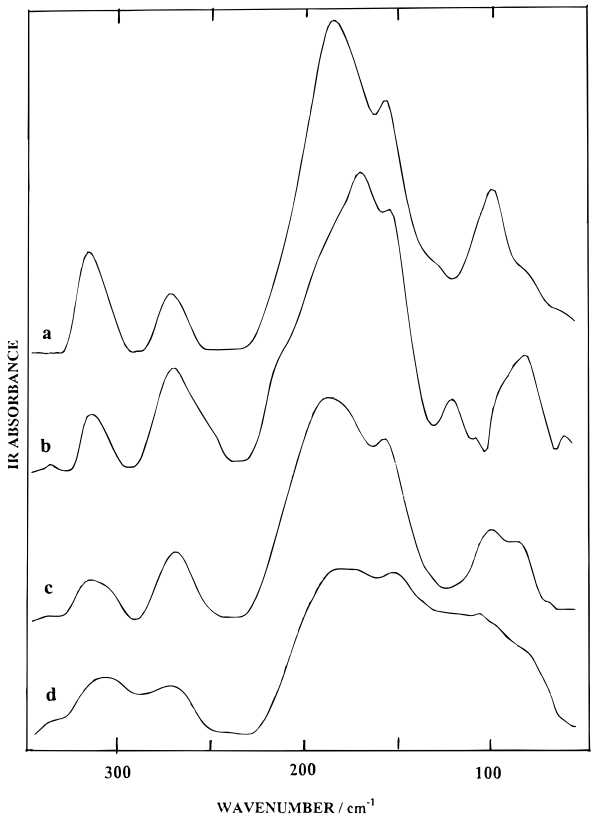

Figure 4. Experimental far-IR spectra of calcined zeolites: (a) Na_{20}-EMT after hydration-dehydration treatment, (b) Na_{20}EMT, (c) Na_{40}-FAU after hydration-dehydration treatment, (d) Na_{40}FAU.

different.[15,19,21−23] The replacement of the Na^+ cations by Li^+, K^+, Rb^+, or Cs^+ produces only slight changes in the position and intensity of the most prominent bands in the stretching and bending regions of the framework. Marked changes are observed in the lower frequency bands assigned to the translatory motions of the extraframework cations. The use of a bolometer detector enables the collection of good quality far-IR spectra of M_{20}EMT samples after hydration−dehydration treatment (Figure 5).

The assignment to translational motions of the cations will be given according to the MD simulations (see below). It is possible to fully convert Na_{20}EMT to $(NH_4)_{20}$EMT via NH_4^+

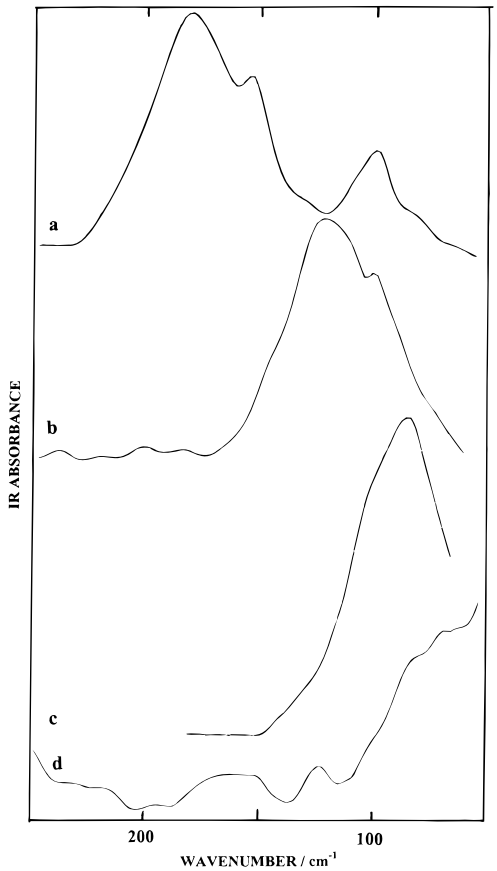

Figure 5. Experimental far-IR spectra of dehydrated M_{20}EMT zeolites: (a) Na_{20}EMT, (b) K_{20}EMT, (c) Rb_{20}EMT, (d) Cs_{20}EMT.

ion exchange.[33] For hydrated $(NH_4)_{20}$EMT sample bands at approximately 1670 cm^{-1} (bending modes of water) and 1430 cm^{-1} (N−H deformation modes of NH_4^+) are observed. The calcination of $(NH_4)_{20}$EMT was monitored up to 773 K by in situ mid-IR spectroscopy. The resulting mid-IR spectrum demonstrates the removing of NH_3 and H_2O and the appearance of two main sharp infrared bands at 3631 and 3545 cm^{-1}.[33] By analogy with FAU zeolites these bands may be assigned to O−H groups stretching in large cages and in the sodalite cages, respectively.[33] In situ thermal deammoniation and dehydration causes the annihilation of the ammonium cation far-IR fingerprint band (160−190 cm^{-1}). The thermal deammoniation product H_{20}EMT exhibits a flat far-IR spectrum below 200 cm^{-1} where only the translatory modes residual Na^+ cations are however still observable at 180 and 100 cm^{-1}. Although dealuminated EMT zeolites have previously been reported,[30] no pure and spectroscopically well characterized, dealuminated samples were synthesized in the present work. However, an interesting alternative to obtain dispersely packed Na^+ cations concerns the replacement of Na^+ cations by NH_4^+ to yield $[NH_4]_nNa_{20-n}$EMT over the full stoichiometry range ($n = 0-20$) and finally after deammination of the latter to yield H_n-Na_{20-n}EMT. At intermediate levels of exchange the two main far-IR features around 200 and 100 cm^{-1} decrease simultaneously with some frequency shifts and some relative intensity changes as previously reported for the FAU zeolites.[51]

2. Raman Scattering Spectra. The mid-frequency Raman spectra of the dehydrated M_{20}EMT zeolites exhibit weak broad bands in the asymmetric (850−1350 cm^{-1}) and the symmetric (650−850 cm^{-1}) Si−O and Al−O stretching regions. In contrast, prominent and sharp bands are observed in the bending region, Figure 6.

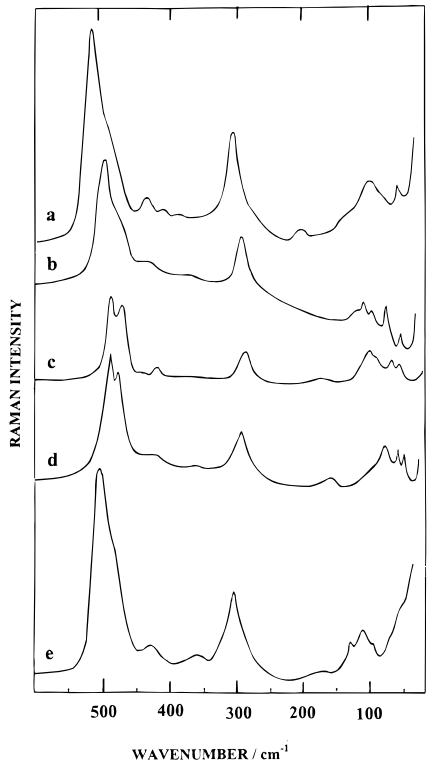

Figure 6. Experimental Raman spectra of dehydrated M_{20}EMT zeolites (exciting radiation, 568.2 nm): (a) Li_{20}EMT, (b) Na_{20}EMT, (c) K_{20}EMT, (d) Rb_{20}EMT, (e) Cs_{20}EMT.

The most intense bands around 500 cm^{-1} are mainly of O−Si(Al)−O bending character, whereas the bands at lower frequency can be assigned to normal modes which can be described in terms of O−Si(Al)−O and Si(Al)−O−Si bending modes as well as Si−O−Si(Al)−O deformation modes. The weak frequency shifts and intensity changes can be attributed to slight structural changes of the framework upon exchange of the extraframework Na^+ cations as it was already proved for the FAU topology by X-ray diffraction.[52] It is interesting to notice that the corresponding cubic M_{56}FAU zeolite Raman spectra ($M^+ = Li^+$, Na^+, K^+, Rb^+, and Cs^+) are analogous, respectively.[25] The problem of the splitting of the most prominent Raman band near 500 cm^{-1} is striking and could not be explained for the FAU structure through variations of structural parameters only.[53] No clear correlation was obtained between the position of the most prominent bands and the Si−O−Si(Al) angle values deduced by diffraction techniques.[25] Due to the lack of experimental structural data, such correlation cannot be established either for the M_{20}EMT zeolites, but the explanation of this spectral behavior is probably the same for both FAU and EMT structures. Indeed, the splitting of the Raman band around 500 cm^{-1} is more evident for both M_{20}EMT and M_{56}FAU with ($M = K^+$ and Rb^+), and the M_{20}EMT and M_{56}FAU spectra are analogous with the corresponding cation.

The supplementary degrees of freedom introduced by the translation motions of the charge balancing cations in sites I'_a, II_a, I'_b, and II_b are expected to be seen by Raman scattering according to the factor group analysis, Table 2. Because of their weak Raman cross sections, the M^+ vibrational motions are weakly apparent on the Raman spectra and often masked by the Raman active deformation modes of the framework. At first, the replacement of the Na^+ cations by Li^+, K^+, Rb^+, Cs^+, and H^+ produces changes in the position and intensity of the most prominent bands near 500 and 300 cm^{-1} and assigned to framework motions (Figure 6). In contrast, the low-frequency

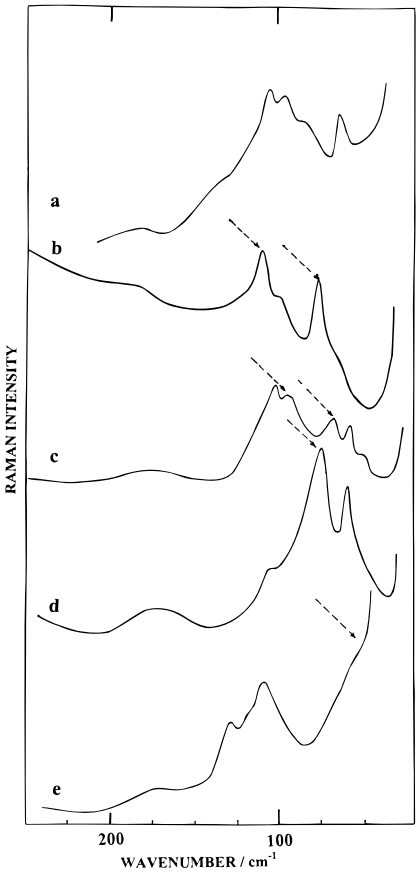

Figure 7. Experimental low-frequency Raman spectra of dehydrated M_{20}EMT zeolites (exciting radiation, 568.2 nm): (a) Li_{20}EMT, (b) Na_{20}EMT, (c) K_{20}EMT, (d) Rb_{20}EMT, (e) Cs_{20}EMT. The arrows indicate the modes mostly sensitive to the cationic degrees of freedom.

bands which are the most sensitive in frequency to the cation exchange, are assigned to modes involving the translational motions of the extraframework cation against the framework, Figure 7.

No significant Raman bands sensitive to the cation exchange are observed in the spectrum of the Na_{20}EMT in the region around 200 cm^{-1}, where the most prominent infrared active Na^+ translational motions are observed. The low-frequency Raman spectra of Na_{20}EMT and Na_{40}FAU were found to be analogous and the cation sensitive modes of the Na^+ cations are observed at 115 and 75 cm^{-1}. The thermally deammoniated product H_{20}EMT exhibits low-frequency Raman bands in the 100 cm^{-1} range, straigthforward assigned to deformation modes of the framework as previously reported for H_{56}FAU.[25,43]

3. MD Calculations. *Vibrational Motions of the EMT Framework.* Spectrum calculations have previously performed for a variety of zeolites using normal modes analyses[19,26,28,51] and MD calculations.[21,22,26,28,37,49] Particularly, the structures of the sodalite, the A-type zeolite and the cubic FAU faujasite have been reproduced accurately using analogous force fields whereas the simulated infrared, Raman, and spectral densities of the atomic motions spectra have good resemblance with the experimental infrared absorption,[15,23] Raman scattering,[25] and inelastic neutron scattering experimental spectra, respectively.[20]

The performed MD simulations permit to bring the M_{20}EMT zeolite structures ($n = 0$ or 20; $M = Na^+$ or K^+) and the vibrational properties in relation. The vibrational spectra do not only depend on the framework topology but also on the Si/Al ratio, the Si/Al distribution, and on the nature of the extraframework cations. The agreement between experimental and present calculated structural parameters of Na_{20}EMT is quite accurate for the harmonic model. We are concerned with small amplitude vibrations close to the energy minimum only. The distribution functions of the atomic positions of the M_nEMT zeolite are all found to be unimodal and Gaussian-like. The Si(Al)−O distances hardly change with the aluminum content ($n = 0$ or 20) and $M = Na^+$ or K^+. However the Si(Al)−O−Si and O−Si(Al)−O angle distributions are sensitive to n ($n = 0$ or 20) but remain practically unchanged with the nature of the cation ($M = Na^+$ or K^+). Although the mean value of the O−Si(Al)−O angles is found to be 109.5°, the distribution is broader for $n = 20$ than that for $n = 0$. This broadening also exists in the Si(Al)−O−Si angle distributions with an asymmetric distribution around the mean value 143° ($n = 20$ and $M = Na^+$ or K^+), whereas the distribution function is found to be Gaussian-like for siliceous EMT ($n = 0$) with 141° as mean value. These results indicate the stability of these M_nEMT ($M = Na^+$ or K^+; $n = 0$ or 20) structures within force field approximation.

The dynamical features of the EMT frameworks can be described from the spectral densities of the atomic motions. However, a better comparison between the simulated dynamic and the experimental features is achieved through the calculated IR absorption and Raman scattering spectra. The absorbance of the infrared spectra are calculated by Fourier transformation of the total dipole moment autocorrelation function (see calculation section). The relative values of the atomic charges mainly influence the intensities in the spectra and in a less extent the frequencies. The zoned Si/Al ordering model[44] generates broader calculated infrared bands than a random Si/Al distribution, particularly in the mid-IR region. The calculated bandwidths using the zoned Si/Al ordering are in better agreement with the experimental results than the random Si/Al ordering, but they do not exclude the possibility of other ordering schemes.[47] Further, the quality of the agreement can include other sources of broadening like the dispersion of some modes.

The Figures 8 and 9 show the calculated IR absorption spectra of M_nEMT ($M = Na^+$ or K^+; $n = 0$ or 20) in the regions 1550−500 cm^{-1} and 700−100 cm^{-1} ranges, respectively. The infrared absorption spectra of some dealuminated EMT zeolite samples are available in the literature[42] and have good resemblances with the calculated spectra. The overall agreement between the calculated and experimental infrared absorption spectra of M_nEMT zeolites is quite satisfactory. Most of the main infrared bands are reasonably reproduced, particularly in the ν_a(Si/Al−O) (1100 cm^{-1}), ν_s(Si/Al−O) (800 cm^{-1}) stretching region, as well as in the δ(Si/Al−O−Si) and δ(O−Si/Al−O) deformation region (600−300 cm^{-1}). No attempt was made to calculate the vibration states of the hydrogen atom of the H_{20}EMT zeolite. It was recently reported that the δ(O−H) and γ(O−H) modes occur at 1129 and 220 cm^{-1} in H_nFAU zeolite, respectively.[54]

The Raman spectra are calculated by Fourier transformation of the total bond polarizability tensor autocorrelation function (see calculation section). A comparison of the simulated and experimental Raman scattering spectra of M_nEMT ($M = Na^+$ or K^+; $n = 0$ or 20) is presented in Figure 10 in the 0−600 cm^{-1} range where the most prominent Raman bands occur. In addition, the weak Raman features around 1100 and 800 cm^{-1} are reasonably reproduced, Table 4.

The frequencies of the spectra are well reproduced in the calculations. Bearing in mind the simple additive bond model without the transversal component for the calculation the Raman intensities, the distribution of calculated Raman intensities is

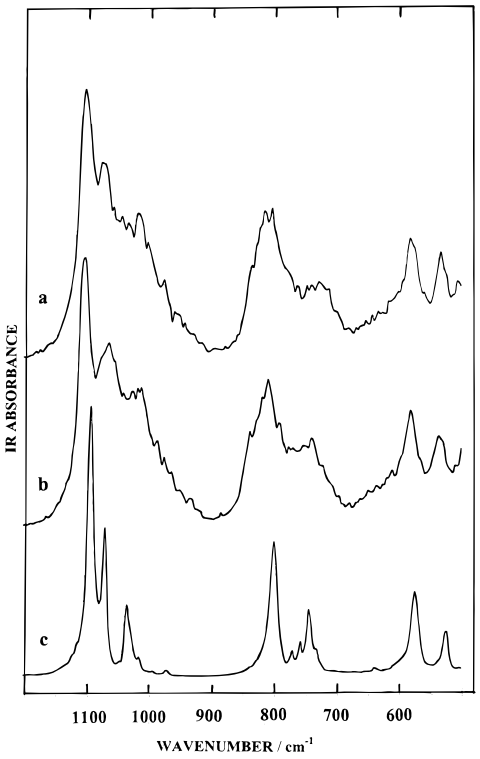

Figure 8. Calculated IR spectra (1200−500 cm^{-1}) of bare EMT zeolites: (a) Na_{20}EMT, (b) K_{20}EMT, (c) EMT.

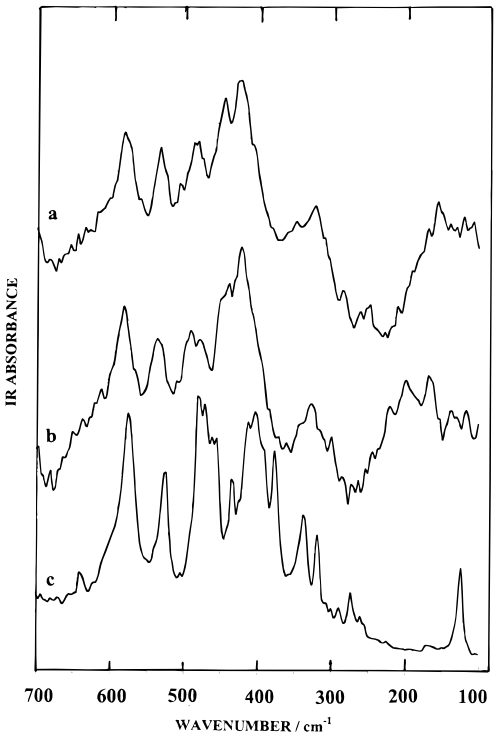

Figure 9. Calculated IR spectra (700−100 cm^{-1}) of bare EMT zeolites: (a) Na_{20}EMT, (b) K_{20}EMT, (c) EMT.

also satisfactory and enables the identification of the modes responsible for the observed bands.

There is, however, one obvious point of discrepancy between the simulated and observed spectra of the M_{20}EMT zeolite. The splitting of the most prominent observed Raman band around 500 cm^{-1} is not reproduced by the simulations. All attempts to reproduce this splitting with alternative force constants within reasonable limits or with variations of structural parameters

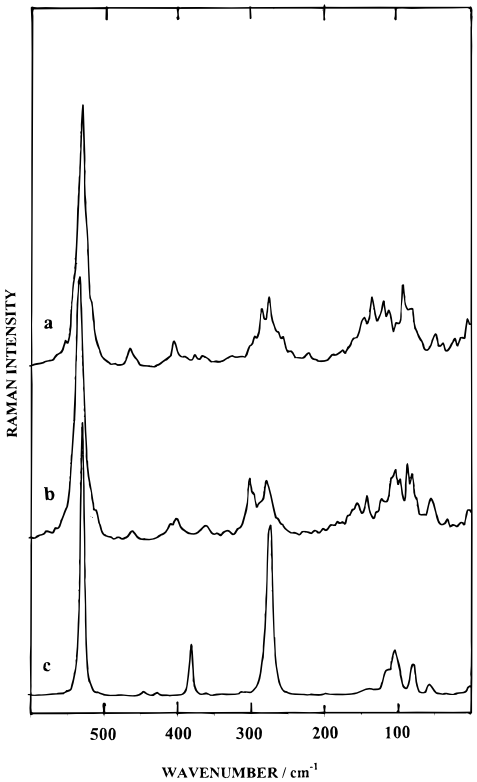

Figure 10. Calculated Raman spectra (600−0 cm^{-1}) of bare EMT zeolites: (a) Na_{20}EMT, (b) K_{20}EMT, (c) EMT.

failed. This splitting could therefore be attributed to processes not considered in the simulation like LO−TO splitting or Fermi resonance.[55] The longitudinal optic (LO)−transversal optic (TO) splitting is a property of dipolar nonzero-wavevector modes of noncentrosymmetric lattices, both the LO and TO components are Raman active. The MD calculations with periodic boundary conditions is restricted to the zero-wavevector modes of the simulation box and does not calculate the LO modes and thus cannot reproduce the Raman feature around 500 cm^{-1}, if it is caused by such a process.

Cation Motions. The calculated densities of vibrational states (DVS) indicate that the cation motions are involved in lattice frequencies up to 400 cm^{-1} for M_{20}EMT ($M^+ = Na^+$ or K^+). However, the main amplitudes of Na^+ cations appear as broad features centered around 100 and 200 cm^{-1} for the Na_{20}EMT zeolite (Figure 11d).

The most significant low-frequency infrared absorption bands are calculated at 90, 135, 170, and 208 cm^{-1} by Fourier transformation of the total dipole moment autocorrelation function. This finding is in reasonable agreement with the experimental far-infrared spectrum (76, 95, 151, and 182 cm^{-1}) (Figure 5). The experimental IR spectrum of *K* species appear as a broad feature centered at 110 cm^{-1} for the K_{20}EMT zeolite whereas the calculated spectrum contains at least 6 bands (81, 107, 138, 164, and 181 cm^{-1}) centered around 126 cm^{-1}. The general agreement is good with a mean error of the order of 12 and 15% for Na and K, respectively. The systematical shift of the calculated spectra to higher frequencies indicates an overestimation of the Coulombic intermolecular potentiel caused by inacurrate charges which were just transferred without fitting from previous calculations of zeolite A.[49] The fact that the calculated spectra are better resolved that the experimental ones indicates a higher order in the models than in the samples. Unfortunately, these results cannot be improved by the analysis of the low-frequency Raman spectra because the applied bond-

TABLE 3: Mean Values and Full Width at Half Height of the Diameter and Area of the Circular and Elliptic Windows of the Calculated EMT, Na_{20}EMT, and K_{20}EMT Zeolite

	circular windows				elliptic windows					
zeolite	diameter/Å		area/Å^2		large axis/Å		small axis/Å		area/Å^2	
EMT[a]	10.15[a]	0.44[b]	81.25[a]	4.75[b]	9.20[a]	0.47[b]	7.20[a]	0.39[b]	52.25[a]	4.38[b]
NaEMT	10.60[a]	0.50[b]	87.75[a]	6.00[b]	9.50[a]	0.60[b]	6.50[a]	0.63[b]	48.25[a]	6.92[b]
KEMT	10.30[a]	0.57[b]	84.50[a]	7.00[b]	9.31[a]	0.56[b]	6.70[a]	0.71[b]	48.75[a]	5.92[b]

[a] Mean values. [b] Full width at half height.

TABLE 4: Characteristic Experimental and Calculated Frequencies of the Infrared and Raman Spectra of the EMT, Na_{20}EMT, and K_{20}EMT Zeolites

	EMT	Na_{20}EMT		K_{20}EMT	
zeolite assignment	calcd (cm^{-1})	exptl (cm^{-1})	calcd (cm^{-1})	exptl (cm^{-1})	calcd (cm^{-1})
ir: ν_a Si(Al)−O	1045, 1080, 1102 s	986−1155 s	1020−1128 s	1014−1152 s	1020−1028 s
R: ν_a Si(Al)−O	1044, 1076 w		1010−1100 w		1026−1096 w
ir: ν_s Si(Al)−O	752, 810 m	738−807 m	750−830 m	738−807 m	730−848 m
R: ν_s Si(Al)−O	746, 772, 800 w		750−830 w		734−830 w
R: δ O−Si(Al)−O	520 s	495 s, 470 sh	520 s	480 s, 450 s	525 s
ir, cations		180 br, 110	200−100	110 br	150−80
R, windows	110, 85, 60 m	110−50 m	110−50 m	110−50 m	110−50 m

[a] ir: infrared. R: Raman. s: strong. m: medium. w: weak. br: broad. sh: shoulder.

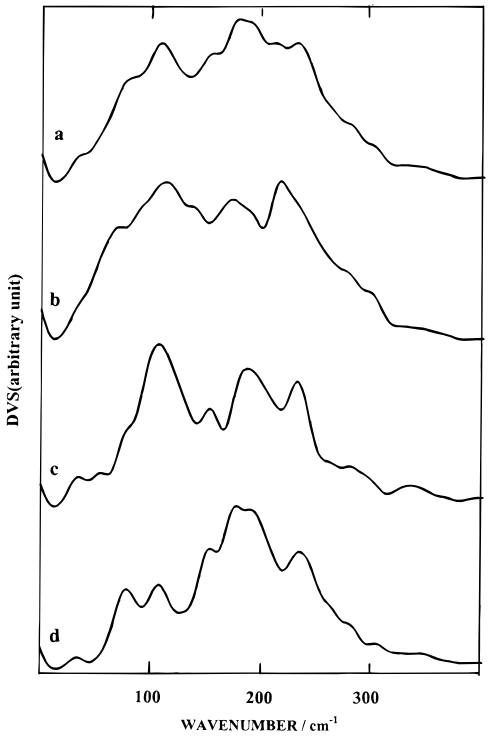

Figure 11. Calculated density of vibrational states of Na^+ in Na_{20}-EMT: (a) site I'_a, (b) site II_b, (c) site II_a, (d) total.

polarizability does not contain any term for the electrostatically interacting cations, so that their degrees of freedom do not contribute to the calculated Raman spectra.

An animation of the atomic motion in the system shows that the cations follow the motions of the framework; this leads to a "softening" of the vibrations of the cations. This finding demonstrates that the far surrounding has an influence on the cation vibrational spectra, as previously reported for zeolite A and cubic M_nFAU.[26,28,49] To test whether it is possible to assign bands to a specific cation sites we have computed the DVS for the cations separately in each crystallographic position. All the DVS are shown in Figure 11.

For the sites I'_a, II_a, and II_b with significant site occupancy the DVS are smeared between 50 and 300 cm^{-1} so that no peak can be assigned exclusively to one particular site. If these results are extrapolated to experimental far-IR and Raman spectra it is possible to say that no observed band represents a single site. This finding is analogous to previously reported results concerning M_nA and M_nFAU zeolites.[26,28,49]

The far-IR spectra as well as low-frequency Raman spectra do not lead to direct site-specific cation information. A rapid overview of the available vibrational spectroscopic results concerning the zeolites with sodalite building blocks and densely and dispersely packed cations can provide some explanation.[15,51]

In situations of high Si/Al ratios and well dispersed cations, correlation effects between cations can be expected to be minimized and a local mode analysis gains in validity. The far-IR spectra of the dealuminated Na_nFAU ($n = 0-56$) and exchanged $H_{56-n}Na_n$FAU have previously been recorded.[15] The removing of the Na^+ cation leads to the decrease of both the prominent IR features around 190 and 100 cm^{-1} and the disappearance of the supplementary shoulders. Recent MD calculations of the DVS of the Na^+ cations in sites I, I′, and II of dealuminated FAU zeolites reveal the same trends.[56] Particularly with dispersed cations ($n<10$), the DVS of Na^+ cations in sites I, I′, and II exhibit both prominent contributions around 100 and 200 cm^{-1} with analogous frequency for all the sites, Figure 12.

So the surroundings of the sites I, I′, and II appear analogous and the large separation between the translational motion of Na^+ cation perpendicularly to the plane of the six-ring assigned around 100 cm^{-1} and the degenerate cation motions parallelly to the plane of the six-ring, around 200 cm^{-1}, is characteristic for the site and nearly nonsensible to long-range crystal effects.

Supplementary maxima of the DVS are calculated in Na_nFAU with $n > 20$, Figure 12. They provide evidence of the dynamic Na^+-Na^+ interactions for more densely packed Na^+ cations. These simulated results are supported by far-IR and low-frequency Raman results. The analogy between the calculated DVS spectra of Na_{32}FAU (Figure 12c) and Na_{20}EMT (Figure 11d) should be noted which also corroborates the influence of the local environment. In the time scale of the MD simulations no cation jump between the sites was observed. It has previously been shown that both ionic conductivity[55] and dielectric relaxation[58] are due to cationic site jumps in FAU zeolites. Moreover, it was demonstrated that these jumps are highly correlated; each jump provokes a redistribution of the surround-

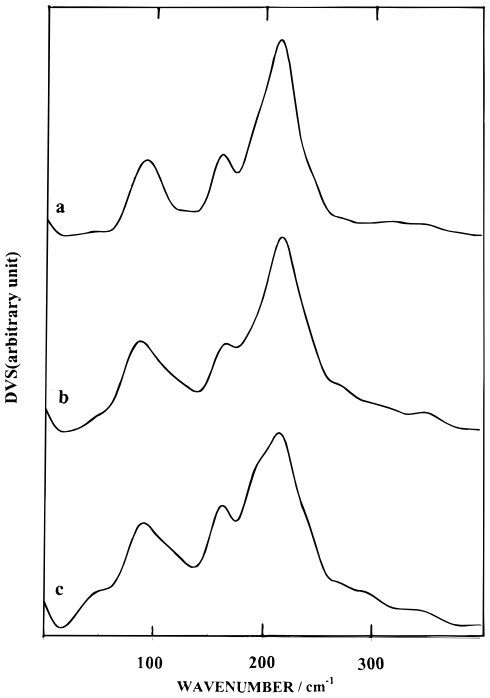

Figure 12. Calculated density of vibrational states of Na^+ (sites I, I′, II): (a) Na_9FAU, (b) Na_{18} FAU, (c) Na_{32} FAU.

ing cations. The collective motions of the cations occur in a microscopic volume including approximately 10 cations. The lifetime of the equilibrium configuration was found to be more than 10^{-6} s, which is a long time compared to the present MD simulations.

Windows Motions. With respect to further investigations of zeolite EMT/sorbate systems we are specially interested in the flexibility of the inner void space. In this context the most important aspect seems to be the flexibility of the windows connecting two adjacent cages.[21,42,43] The windows are the smallest sections of the inner void space, they have to be passed by diffusing molecules and therefore can be considered as a transition-state region for diffusion processes. Even small deformations of the window size may lead to drastic changes of the activation energies if the dimensions of the sorbates are similar to the size of the windows. There are no direct experimental data on the extent of motion of the atoms in zeolite materials. The isotropic thermal parameter deduced in fitting measured diffraction data[5] is a measure of the thermally induced departure of an atom from its equilibrium position, being related to the mean square displacement, $\langle u^2 \rangle$, by $B = 8\pi^2\langle u^2 \rangle$. The diffraction data for calcined EMT at 50 K yield a value for the framework oxygen atoms of $B = 1.9$ Å^2 corresponding to $\langle u^2 \rangle = 0.024$ Å^2.[5] This B value which was constrained to be equal for all the oxygen atoms is typical of those reported in similar zeolite crystal structure refinements. The MD calculations were not carried out at 50 K in the present work, but according to previous works concerning the Na_{56}FAU zeolite the $\langle u^2 \rangle$ values deduced from diffraction data were generally found to be larger than the calculated ones.[21] This is not surprising, for the nature of the diffraction data fitting is such that the optimized B-factor values typically compensate for a variety of other complicating factors present in the material, such as the effects of framework aluminum, defects, disorder, and inhomogenity.[53]

Although the extraframework cations of M_nEMT zeolites are not found to be located in the windows of the framework, as for the A zeolites, the calculated dimensions of the windows of M_nEMT zeolites were found to be dependent both on the aluminum content and on the presence of cations and on their sizes. According to the size of cations, the effects of cations are different on the two kinds of windows. At room temperature, the MD calculations yield substantial departures of the framework atoms from their equilibrium positions. Inspection reveals that these changes largely result from reorientational motion of successive tetrahedra by rotations about the Si/Al−O bonds. The distribution of the diameter of the circular window and of the main axes of the elliptic window through selected O−O distances are presented in the Figures 13 and 14, respectively. These values are pure structural parameters obtained from geometrical calculations. It will be necessary to consider the van der Waals radii of the atoms in order to transfer these results to the interpretation of diffusion processes. The mean values and the full width at half-height (fwhh) of these lengths and of the area of the windows are listed in Table 3.

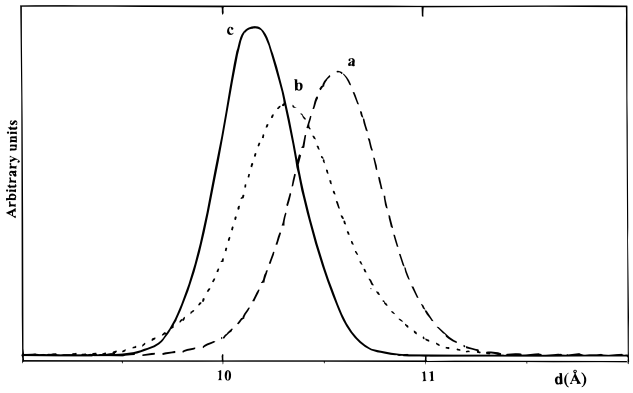

Figure 13. Distribution function of the circular window diameter: (a) Na_{20}EMT, (b) K_{20}EMT, (c) EMT.

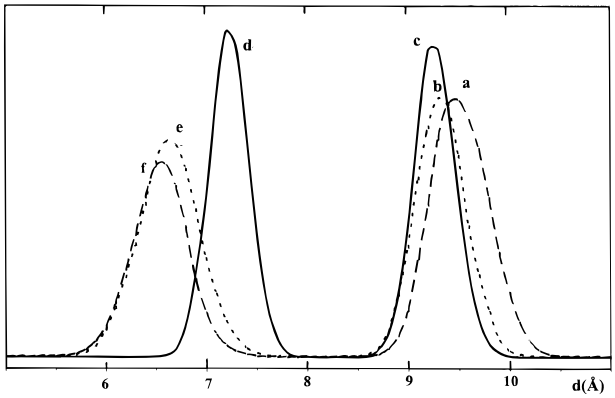

Figure 14. Distribution function of the elliptic window axis; large axis: (a) Na_{20}EMT (b) K_{20}EMT, (c) EMT. Small axis: (d) EMT, (e) K_{20}EMT, (f) Na_{20}EMT.

The circular windows are situated between two supercages and form the superchannel. In the siliceous EMT the mean diameter is 10.15 Å with an area of 81.25 Å^2. Globally, when the structures contain cations and aluminum, the mean diameter and the mean area increase. We can also observe a light broadening of these distributions (Figure 13). It is interesting to notice that the nature of the cation has an influence on these distributions. The mean diameter is larger with sodium than with potassium (10.6 and 10.3 Å, respectively). On the contrary, the fwhh is larger for potassium (Na: 0.50 Å and K: 0.57 Å).

In the siliceous EMT the main axes D and d of the elliptic window have the values 9.20 and 7.20 Å, respectively (Figure 14), and the area is 52.25 Å^2. When the structures contain aluminum and cations, the area of the window decreases. We can notice that the elliptic windows are flattened by the presence

of cations: the ratio d/*D* decreases. The effects of aluminum content and cations on the large axis *D* are the same as observed for the circular windows. On the contrary these effects are inverted for the small axis *d*. Although the cations are not located in the windows, their presences have a drastic influence on the aperture of the windows.

To obtain information about the frequencies involved in the window fluctuations, the spectral density was computed as Fourier transformation of the diameter autocorrelation function (see Experimental Section). The spectral densities of the diameter and axis fluctuations of siliceous EMT display the most intensive peaks around 100 cm^{-1} although weak contributions appear up to 300 cm^{-1}, see also calculated low-frequency IR and Raman spectra of siliceous EMT which contain no cation in Figures 9c and 10c. The cations loading leads to broadening and weak frequency shifts. The experimental and calculated Raman spectra of M_nEMT zeolites exhibit prominent bands around 100 cm^{-1} (Figures 6 and 9) which have been assigned to the window fluctuations, but will also contain contribution of cationic degrees of freedom.

Conclusions

The infrared absorption and Raman scattering spectra of a series of ion-exchanged bare M_nEMT zeolites ($M = Li^+$, Na^+, K^+, Rb^+, Cs^+, NH_4^+, and H^+) have been recorded and described in the mid and low-frequency regions. Due to the different linking of sodalite cages the microporous structures of the hexagonal M_nEMT and cubic M_nFAU frameworks are substantially different, particularly in the type and size of the pore windows, whereas the main trends of the vibrational properties were found to be analogous with identical aluminum content. However, significant changes in position and intensity of the bands assigned to the framework vibrations were observed according to the nature of the extraframework charge-balancing cation of the exchanged zeolites. Molecular dynamics calculations were used to model the vibrational features of the M_nEMT ($n = 0$ or 20) framework and extraframework cations. Using a zoned model of the Si/Al distribution, the main features of both the IR and Raman spectra were reproduced in the mid as well as in the low-frequency ranges. The results of the calculations demonstrate that the cation vibrations participate in the spectral range from 20 to 250 cm^{-1} for all cation sites and couple with the low-frequency framework motions. The data of the molecular dynamics simulations of the window fluctuations in the M_nEMT zeolites show that the aluminum content and extraframework cations affect both the mean value of the diameter and the amplitude of the fluctuations of the windows in the zeolite although the cations are not located in the windows. The instantaneous geometrical modifications of the windows can play an important role on the selectivity of the diffusion of molecules through the cages.

Acknowledgment. The authors are very grateful to C. Bodelot and Dr A. Lorriaux for their assistance and advice while using far-IR and Raman instruments, respectively. The authors acknowledge Dr P. Bornhauser and Dr K. S. Smirnov for helpful discussions. Computing time at IDRIS (Project 940145) is acknowledged. The Centre d'Etudes et de Recherches Lasers et Applications (CERLA) is supported by the Ministère chargé de la recherche, the Région Nord/Pas de Calais, and the Fonds Européen de Développement Economique des Régions.

References and Notes

(1) Szostak, R. *Introduction to Zeolite Science and Practice, Studies in Surface Science and Catalysis*; van Bekkum, H., Flanigen, E. M., Jansen, J. C., Eds.; Elsevier Sciences Publishers B. V.: Amsterdam, The Netherlands, 1991; Vol. 58, pp 153−199.

(2) Delprato, F.; Delmotte, L.; Guth, J. L.; Huve, L. *Zeolites* **1990**, *10*, 546.

(3) Dougnier, F.; Patarin, J.; Guth, J. L.; Anglerot, D. *Zeolites* **1992**, *12*, 160.

(4) Burkett, S. L.; Davis, M. E. *Microporous Mater*. **1993**, *1*, 265.

(5) Baerlocher, C.; McCuster, L. B.; Chiapetta, R. *Microporous Mater*. **1994**, *2*, 269.

(6) Lievens, J. L.; Verduijn, J. P.; Bons, A. J.; Mortier, W. J. *Zeolites* **1992**, *12*, 698.

(7) Feijen, E. J. P.; De Vadder, K.; Bosschaerts, M. H.; Lievens, J. L.; Martens, J. A.; Grobet, P. J.; Jacobs, P. A. *J. Am. Chem. Soc*. **1994**, *116*, 2950.

(8) Van Koningsveld, H. *Introduction to Zeolite Science and Practice, Studies in Surface Science and Catalysis*; van Bekkum, H., Flanigen, E. M., Jansen, J. C., Eds.; Elsevier Sciences Publishers B. V.: Amsterdam, The Netherlands, 1991; Vol. 58, pp 13−33.

(9) Meier, W. M.; Olson, D. H. *Atlas of Zeolite Structure Types*; Butterworth-Heinemann; Surrey, U.K., 1992; pp 88 and 96.

(10) Mortier, W. J. *Compilation of Extraframework Sites in Zeolites*; issued by the Commission of the International Zeolite Association, 1981.

(11) Thomas, J. M.; Ramdas, S.; Millword, G. R.; Klinowski, J.; Audien, M.; Gonzalez-Calbet, J.; Fyfe, C. A. *J. Solid State Chem.* **1982**, *45*, 368.

(12) Martens, J. A.; Jacobs, P. A.; Cartligde, S. *Zeolites* **1989**, *9*, 423.

(13) Fitch, A. N.; Jobic, H.; Renouprez, A. *J. Phys. Chem*. **1986**, *90*, 1311.

(14) Engelhardt, G.; Michel, D. *High-Resolution Solid State NMR of Silicates and Zeolites*; John Wiley & Sons: New York, 1987.

(15) Godber, J.; Ozin, G. A. *J. Phys. Chem*. **1988**, *92*, 2841.

(16) Dutta, P. K.; Twu, J. *J. Phys. Chem*. **1991**, *95*, 2498.

(17) Czjek, M.; Jobic, H.; Fitch, A. N.; Vogt, T. *J. Phys. Chem*. **1992**, *96*, 1535.

(18) Lievens, J. L.; Mortier, W.J.; Chao, K. J. *J. Phys. Chem. Solids* **1992**, *53*, 1163

(19) de Man, A. J. M.; van Santen, R. A. *Zeolites* **1992**, *12*, 269.

(20) Jobic, H. *Spectrochim. Acta* **1992**, *48A*, 293.

(21) Schrimpf, G.; Schlenkrich, M.; Brickmann, J.; Bopp, P. *J. Phys. Chem.* **1992**, *96*, 7404.

(22) Smirnov, K. S.; Bougeard, D. *J. Phys. Chem.* **1993**, *97*, 9434.

(23) Jacobs, W. P. J. H.; van Wolput, J. H. M. C.; van Santen, R. A. *Zeolites* **1993**, *13*, 170.

(24) Engelhardt, G.; Hunger, M.; Koller, H.; Weitkamp, *J. Stud. Surf. Sci. Catal*. **1994**, *84*, 412.

(25) Brémard, C.; Le Maire, M. *J. Phys. Chem.* **1993**, *97*, 9695.

(26) Krause, K.; Geidel, E.; Kindler, J.; Förster, H.; Böhlig, H. *J. Chem. Soc., Chem. Commun.* **1995**, 2481.

(27) Olson, D. H. *Zeolites* **1995**, *15*, 439.

(28) Krause, K.; Geidel, E.; Kindler, J.; Förster, H.; Smirnov, K. S. *Vib. Spectrosc*. **1996**, *12*, 45.

(29) Demontis, P.; Suffriti, G. B. *Chem. Rev*. **1997**, *97*, 2845 and references therein.

(30) Li, H.-X.; Annen, M. J.; Chen, C.-Y.; Arhancet, J. P.; Davis, M. E. *J. Mater. Chem.* **1991**, *1*, 79.

(31) Alfredson, V.; Ohsuna, T.; Terasaki, O.; Bovin, J. O. *Angew. Chem., Int. Ed. Engl*. **1993**, *32*, 1210.

(32) Hunger, M.; Engelhardt,; G. Koller H.; Weitkamp, J. *Solid State Nucl. Reson.* **1993**, *2*, 111.

(33) Su, B. L.; Manoli, J. M.; Potvin, C.; Barthomeuf, D. *J. Chem. Soc., Faraday Trans.* **1993**, *89*, 857.

(34) Martens, J.A.; Xiong, Y. L.; Fedjen, E. J. P.; Grobet, P. J.; Jacobs, P. A. *J. Phys. Chem.* **1993**, *97*, 5132.

(35) Brémard, C.; Le Maire, M.; Manoli, J. M.; Potvin, C. *Stud. Surf. Sci. Catal.* **1994**, *84*, 1027.

(36) Wu, C. N.; Chao, K. J. *J. Chem. Soc., Faraday Trans*. **1995**, *91*, 167.

(37) Brémard, C.; Bougeard, D. *Adv. Mater*. **1995**, *7*, 10 and references therein.

(38) Murphy, D.; Massiani, P.; Franck, R.; Barthomeuf, D. *J. Phys. Chem.* **1996**, *100*, 6731.

(39) Bougeard, D.; Brémard, C.; Dumont, D.; Le Maire, M.; Manoli, J. M.; Potvin, *J. Mol. Struct.* **1997**, *410−411*, 375.

(40) Chen, N. Y.; Degnan, Jr, T. F.; Smith, C. M. *Molecular Transport and Reaction in Zeolites, Design and Application of Shape Selective Catalysts*; VCH Publishers: Weinheim, Germany, 1994.

(41) Su, B. L.; Norberg, V. *Langmuir* **1998**, *14*, 2352.

(42) Deem, M. W.; Newsam, J. M.; Creighton, J. A. *J. Am. Soc. Chem.* **1992**, *114*, 7198.

(43) Smirnov, K. S.; Bougeard, D. *Zeolites* **1994**, *14*, 203.

(44) Feijen, E. J. P.; Lievens, J. L.; Martens, J. A.; Grobet, P. J.; Jacobs, P. A. *J. Phys. Chem.* **1996**, *100*, 4970.

(45) Herrero, C. P.; Ramirez, R. *J. Phys. Chem.* **1992**, *96*, 2246.

(46) van Dun, J. J.; Mortier, W. J. W. *J. Phys. Chem.* **1988**, *92*, 6740.

(47) Melchior, M. T.; Vaughan, D. E. W.; Pictroski, C. F. *J. Phys. Chem.* **1995**, *99*, 6128.
(48) van Dun, J. J.; Dhaeze, K.; Mortier, W. J.; Vaughan, D. E. W. *J. Phys. Chem. Solids* **1989**, 50, 469.
(49) Smirnov, K. S.; Le Maire, M.; Brémard, C.; Bougeard, D. *Chem. Phys.* **1994**, *179*, 445.
(50) Smirnov, K. S.; Bougeard, D. *J. Raman Spectrosc.* **1993**, *24*, 258.
(51) Ozin, A. G.; Baker, M. D.; Godber, J.; Gil, C. *J. Phys. Chem.* **1989**, *93*, 2899.
(52) Costenoble, M. L.; Mortier, W. J.; Uytterhoeven, J. B. *J. Chem. Soc., Faraday Trans. 1* **1976**, *72*, 1877.
(53) Creighton, J. A.; Deckman, H. W.; Newsam, J. M. *J. Phys. Chem.* **1994**, *98*, 448.
(54) Ermoshin, V. A.; Smirnov, K. S.; Bougeard, D. *Surf. Sci.* **1996**, *368*, 147.
(55) Decius, J. C.; Hexter, R. M. *Molecular Vibrations in Crystal*; McGraw-Hill: New York, 1977.
(56) Dumont, D. Thesis, Lille, 1996.
(57) Jansen, F. J.; Schoonheydt, R. A. *J. Chem. Soc., Faraday Trans. 1* **1973**, *69*, 1338.
(58) Carru, J. C.; Tabourier, P.; Wacrenier, J. M. *J. Chem. Phys.* **1991**, *88*, 307.